PHANTOM VORTICITY IN EULER SOLUTIONS ON HIGHLY STRETCHED GRIDS

S. A. Prince†, D. K. Ludlow, N. Qin
Cranfield College of Aeronautics, Bedfordshire, UK
† Currently DERA Bedford, UK

Keywords: *Phantom vorticity, Numerical dissipation, Euler equations, Grid stretching*

Abstract

The excessive numerical dissipation, which is known to occur when the steady Euler equations are solved on fine, highly stretched grids is investigated. A new formulation of the higher order MUSCL scheme that accounts for grid non-uniformity is derived and applied to the alleviation of this "phantom vorticity".

1 Introduction

Several investigators have shown that numerical solutions of the Euler equations on highly stretched grids past a smooth inclined body can exhibit a numerical boundary layer leading to the development of symmetric leeward side vortices [1][2][3]. The development of this "phantom vorticity" can occur even with the application of a slip boundary condition at the wall.

The inviscid character of the Euler equations means that they cannot account for viscous vorticity generation. Numerical solution of these equations can, however, involve mechanisms for the erroneous generation of vorticity.

In inviscid flow, curved shock waves introduce circulation, entropy layers and vorticity into the solution. Marconi [1] demonstrated that for a conical-Euler solution on a slender cone at angle of attack in a supersonic stream, a curved embedded crossflow shock causes separation of the flow from the cone surface and a vortex to form near the leeward symmetry plane. In addition, since numerical solutions are obtained from approximate or discretised forms of the governing equations, Euler solutions may include vorticity generation by the effect of truncation error – numerical dissipation.

Once a vortex is formed the Euler equations allow for its convection downstream but cannot simulate its diffusion due to physical viscosity. All computational schemes, however, are dissipative and even without the addition of artificial viscosity, will diffuse and destroy vorticity. Numerical dissipation will diminish the strength of vortices, but not in a manner representative of a viscous flowfield.

The accurate capture of boundary layer separation and subsequent vortex development is critical for the computational prediction of the flow past smooth aircraft or missile forebodies. If the errors associated with phantom vorticity are large enough, will they lead to errors in viscous calculations, and if so, what can be done to alleviate its effect?

This paper seeks to address these issues by detailed numerical studies of the supersonic flow about an inclined slender body, and by careful investigation of the solution algorithms used in the flow solver.

2 Previous Investigations

Chinilov [4] investigated the phenomenon of the non-physical, numerical boundary layer that he found to develop near the body surface when a supersonic inviscid stream flows past a blunt body. A steady two-dimensional supersonic flow past a circular cylinder was investigated using several mesh resolutions by use of a first-order finite volume numerical Godunov scheme. Chinilov found that he could reduce the

phantom viscosity by either refining the grid or employing second-order spatial discretisation.

In order to compute a flow solution efficiently and to resolve the boundary layer and associated flow features, grid stretching is often used. Typically a grid is created which is stretched in a wall normal direction such that the cell width is a strictly increasing function of the distance from the wall. Although the previous investigation was performed without any appreciable grid stretching, a number of investigators have shown that grid stretching can have a big effect on the accuracy of modern schemes for compressible fluid flows.

Turkel [5] showed that many popular central difference and upwind methods reduce to first-order spatial accuracy in regions where the grid is highly non-uniform. Various algebraic and exponential grid-stretching functions were investigated. It was found that algebraic stretching was sufficiently smooth to allow second-order techniques to maintain their formal accuracy. Exponential stretching functions however proved to deteriorate the spatial accuracy to first-order unless special weighted formulas are used. In addition it was demonstrated that second-order accuracy could be maintained with these schemes only if the mesh accurately reflects the properties of the solution.

A number of methods have been developed to account for grid stretching and thereby maintain spatial accuracy. Batina [6] developed improved algorithms for spatial and temporal discretisation in his unstructured Euler solver for the investigation of the unsteady aerodynamics of a two-dimensional pitching aerofoil. In particular he developed a simple interpolation of the primitive variables that he employed in the standard MUSCL scheme in order to treat highly skewed tetrahedral cells. This weighted interpolation of the primitive variables was based on the distance between the centroid and the midpoint of the appropriate edge. Batina [7] further developed this technique for three-dimensional flows, this time with a different MUSCL type scheme.

Liou and Hsu [8] developed a high resolution scheme for their time accurate three-dimensional structured finite volume solver based on Roe's upwind technique for flux difference splitting. Non-uniformity of cell sizes was accounted for by deriving a number of factors based on the sizes of each cell in the stencil.

With this information it was decided to investigate the generation of phantom vorticity around a slender, sharp nosed, smooth cylindrical body. In particular, the affect of grid stretching and the spatial accuracy of the solver were studied.

3 Numerical Solver and Grid

The numerical analysis was performed using a three-dimensional time-marching, cell-centred finite volume Navier-Stokes (NS) solver that was operated in Euler mode. The steady compressible Euler equations were solved using a cell-centred finite volume approach within a structured discretised domain. Inviscid fluxes were calculated using Osher's approximate Riemann solver. Higher (second or third) order spatial accuracy was attained by the use of the MUSCL variable extrapolation together with a slope limiter. An approximate solution of the Riemann boundary problem was used to prescribe the Euler slip boundary conditions at the wall. More details about the solver can be found in [9].

A three-calibre tangent-ogive cylinder geometry was chosen for the current numerical investigation. Experimental studies with this geometry inclined at 10 degrees to a Mach 2.0 flow has been carried out at ONERA [10]. The Experimental results revealed a well-developed symmetric vortex pattern on the leeward side of the body.

Five single-block structured grids of varying cell number, were generated around the body. The coarsest "Euler" grid was of size 60× 54×45 and employed near-wall cells of $0.00185D$ radial thickness (D=1 calibre) and a *tanh* radial stretching function. The next four grids, suitable for NS calculations, all used near wall cells of $2\times10^{-4}D$ radial thickness and again employed a *tanh* radial stretching function. The

cells in each grid were spaced uniformly in the circumferential direction.

4 The Effect of Spatial Accuracy and Grid Stretching.

The NS solver was employed in Euler mode to obtain solutions on the five grids (detailed in the key in Figure 1) using the standard MUSCL formulation with a κ factor set for third-order spatial accuracy. It was found that the first two grids converged well down to five orders of magnitude, whereas those on the three finest grids stalled at around 2 to 2.5 orders of residual convergence. The CFL number, initially set to 0.3, was successively reduced to 0.05 in an attempt to converge the solutions further, but was found to have little effect. Analysis of the stalled solutions, checking every 1000 time steps, revealed that the flow structure did not exhibit any appreciable change. Figure 1 presents the five solutions for the circumferential pressure distributions at x/D=7. It would be expected that, as the grid is further refined, the solution would converge to the same circumferential distribution. What is observed, however, is a progressive deviation from the expected solution (curve for grid 1) and the development of pronounced suction peaks due to the resolution of phantom vortices on the leeward side of the body.

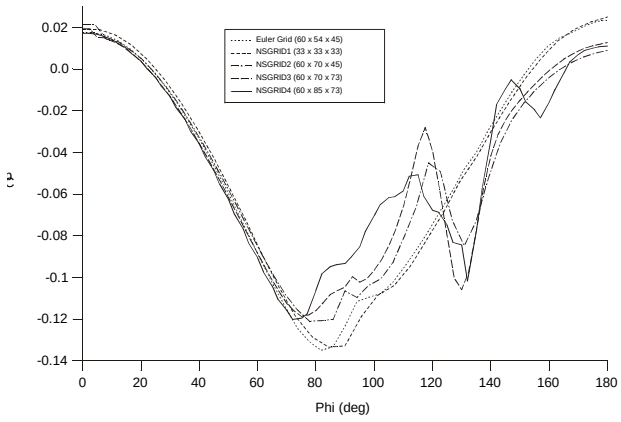

Figure 1: Grid convergence for Euler solutions on five grids using third-order MUSCL scheme.

Figure 2 presents the computational grid and density contours at x/D=8 obtained by the fully converged Euler solution on grid 1. This is the correct flow structure expected of an Euler solution, without any flow separation or leeward side vortices. Close inspection of the crossflow velocity vectors, however, did reveal the presence of a slight velocity profile close to the leeward body surface.

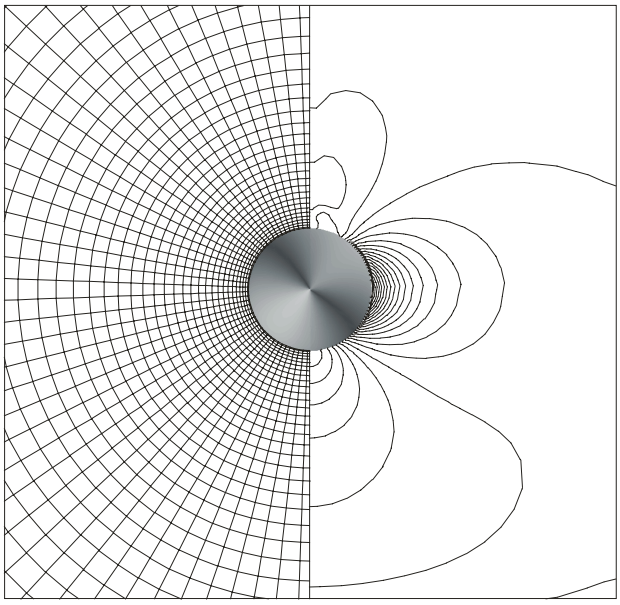

Figure 2: Density contours for third-order MUSCL Euler solution on grid 1.

The corresponding flow solution on the finest NS grid (60×85×73) at the same axial station is presented in Figure 3. Figure 3b) clearly shows a well-developed numerical boundary layer that separates off the leeward side of the body to form a primary, secondary and tertiary vortex system similar to that expected of a viscous solution rather than an Euler solution.

Since the origin of the vorticity is non-physical the resulting vortex pattern does not agree with either experiment or with the laminar NS solution on the same grid. Solutions were also obtained using a different formulation of the Euler wall slip boundary condition and using the Roe Approximate Riemann Solver. None of these changes had any appreciable affect on the solution.

The next step in the investigation was to look at the effect of spatial accuracy. By altering the κ factor in the MUSCL scheme one can obtain second-order spatial accuracy, and by

switching off the MUSCL scheme one can obtain solutions of first-order spatial accuracy. Figure 4 presents the first-order solution at x/D=8. A small numerical boundary layer is still observed on the leeward surface and the flow is seen to separate forming a very small, hardly visible, vortex close to the leeward symmetry plane.

Figure 5 compares the circumferential surface pressure distribution at x/D=7 for the first and third-order accurate solutions on grid 5. The higher order result predicts separation at around ϕ=100^o and two suction peaks associated with a primary and secondary vortex. The first-order solution is much closer to that expected of an Euler solution, with only a slight inflexion at ϕ=150^o indicating a small weak primary vortex.

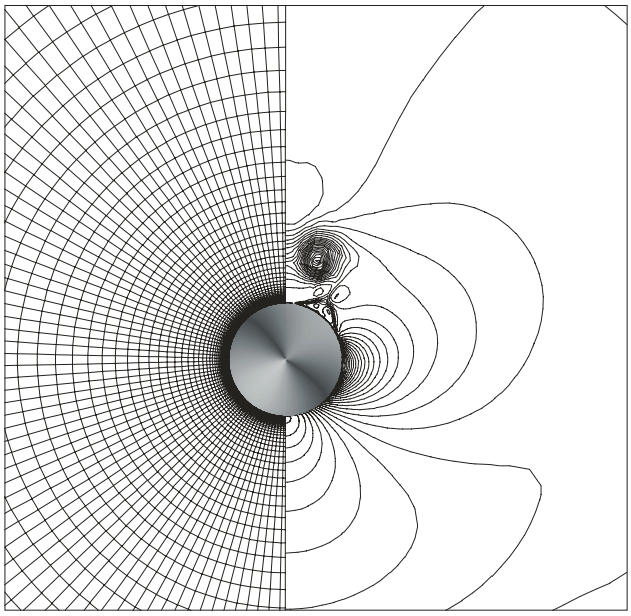

a) Density contours and crossflow plane grid

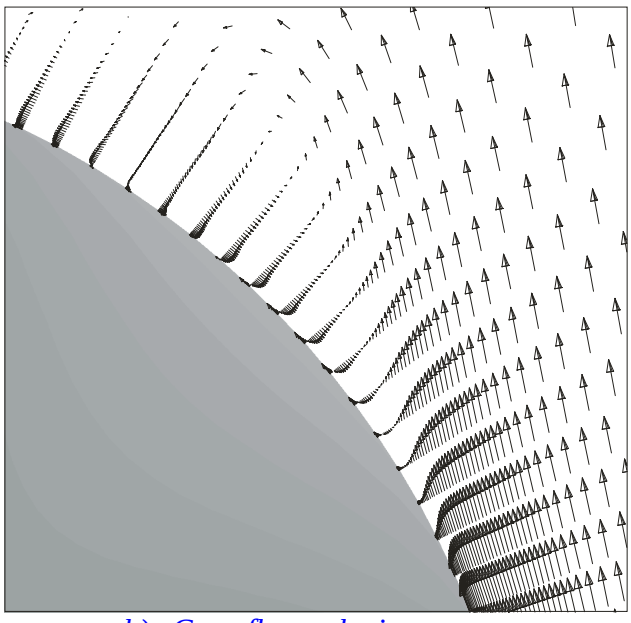

b) Crossflow velocity vectors

Figure 3: Euler third-order MUSCL solution on grid 5.

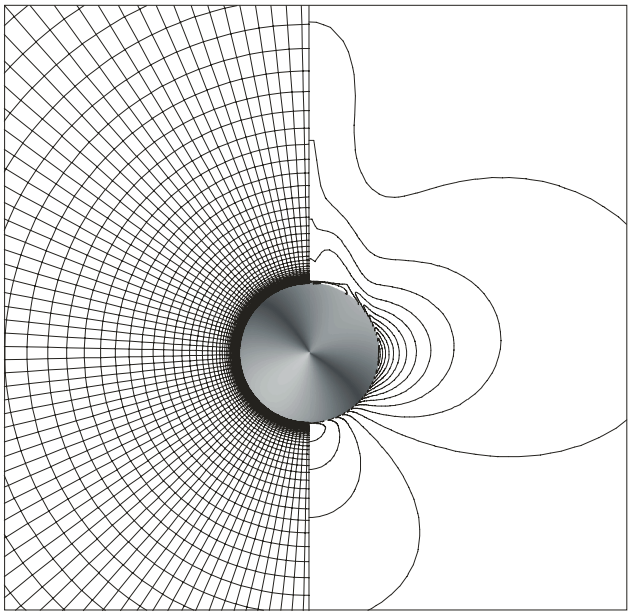

a) Density contours and crossflow plane grid

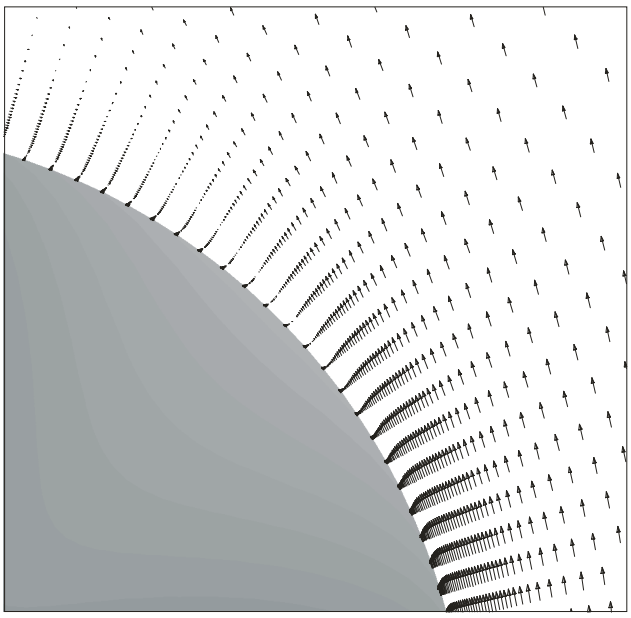

b) Crossflow velocity vectors

Figure 4: Euler first-order MUSCL solution on grid 5.

The third-order value of the pressure coefficient (C_p) at the leeward symmetry plane is equivalent to that predicted in a third-order viscous solution, but that for the first-order solution is over-predicted by $\Delta C_p \approx 0.01$. This can be explained by the overall reduction in spatial accuracy and the corresponding increase in numerical dissipation.

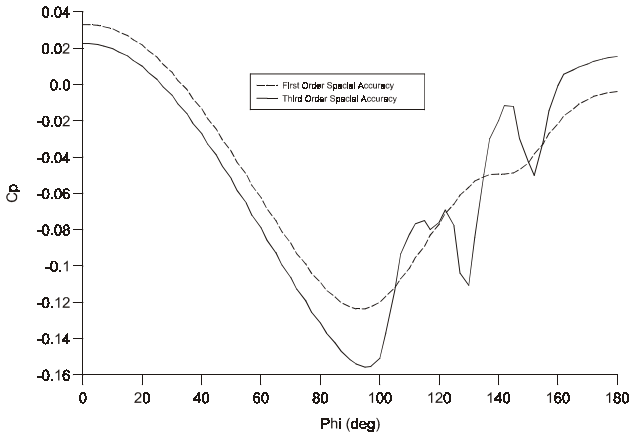

Figure 5: Effect of spatial accuracy on Euler solution on grid 5

A sixth grid was then generated in order to investigate further the effect of grid stretching. Grid 6 (60×140×73), shown in Figures 7 and 8 had a region of cells of identical cell width adjacent to the wall; outside these cells the cell width was increased smoothly, using a *tanh* function, to the freestream boundary. The interface between the uniform and stretched regions of the grid was positioned well beyond the influence of any boundary layer

A third-order MUSCL calculation was performed on grid 6. While the solution no longer contained a numerical boundary layer at the wall, a spurious numerical shear layer was seen to develop from the interface where the cell width began to increase away from the wall. As with the other computations where phantom vorticity was found to develop, the solution could not be fully converged.

Grid 6 was then further modified by pulling the grid stretching interface slightly further away from the wall, introducing more cells into the uniform cell region such that the cell width could be maintained. The numerical shear layer was found to move with the stretching interface. In effect, the numerical boundary layer was moved away from the wall and followed the position of the discontinuity in the gradient of cell width. Again it was noted that the solution could only be converged down to 2.5 orders before the calculation stalled.

This evidence suggests that the excessive numerical dissipation is associated with the localized loss of spatial accuracy when using the standard high resolution MUSCL scheme in regions where the grid is highly stretched. In order to rectify this problem, it was decided to modify the MUSCL scheme to account for grid stretching.

5 A New Formulation of the MUSCL Scheme for Non-Uniform Grids

This section presents the derivation of a high resolution MUSCL scheme that uses a weighted formulation of each cell size in the computational stencil.

The original formulation of the MUSCL scheme [11] was derived from the piecewise quadratic distribution for the variable U in a cell i given by:

$$U = U_i + (x - x_i)\left.\frac{\partial U}{\partial x}\right|_i + \frac{3\kappa}{2}\left[(x - x_i)^2 - \frac{\Delta x^2}{12}\right]\left.\frac{\partial^2 U}{\partial x^2}\right|_i \qquad (1)$$

where U_i is the average value defined by:

$$U_i = \frac{1}{\Delta x}\int_{i-\frac{1}{2}}^{i+\frac{1}{2}} U(x)dx .$$

The original MUSCL scheme assumes that each cell is the same size, i.e., that there is no grid stretching. Figure 6 shows the one-dimensional computational stencil about cell i for a stretched grid. For a non-uniform grid the term Δx in (1)

is equal to the width of cell i denoted by s_i such that:

$$s_i = x_{i+1/2} - x_{i-1/2}. \qquad (2)$$

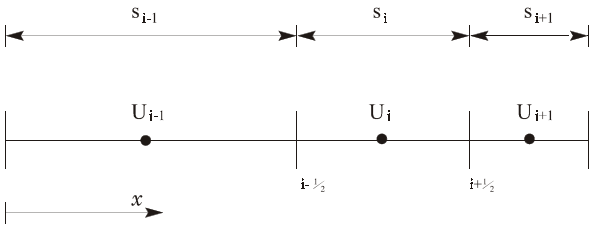

Figure 6: Finite volume representation of stretched grid about cell i.

Taking the function $U(x)$ to be a quadratic function of x of the form:

$$U - U_i = A(x - x_i)^2 + B(x - x_i). \qquad (3)$$

Substituting $x=x_{i\pm1}$ and $U=U_{i\pm1}$ into equation (3) yields two simultaneous linear equations which can be solved for A and B. The derivatives of U with respect to x at $x=x_i$ are then evaluated by differentiation of equation (3). Substituting these derivative terms into equation (1) and setting:

$$r_i^{\pm} = \frac{s_i + s_{i\pm1}}{2s_i} \qquad (4)$$

$$\tilde{\Delta}_i^{\pm} = \pm\frac{1}{r_i^{\pm}}(U_{i\pm1} - U_i) \qquad (5)$$

yields an equation, of the MUSCL form, for the evaluation of the variables at the interfaces of cell i.

For the left-hand side of the interface $i+1/2$, this results in the following relation:

$$U^L_{i+1/2} = U_i + \frac{\phi}{2(r_i^+ + r_i^-)}\left((r_i^- + \kappa\phi)\tilde{\Delta}_i^+ + (r_i^+ - \kappa\phi)\tilde{\Delta}_i^-\right) \qquad (6)$$

The corresponding expression for the values on the right hand side of the interface $i+1/2$ (by a similar treatment for the cell $i+1$) gives:

$$U^R_{i+1/2} = U_{i+1} - \frac{\phi}{2(r_{i+1}^+ + r_{i+1}^-)}\left((r_{i+1}^- - \kappa\phi)\tilde{\Delta}_{i+1}^+ + (r_{i+1}^+ + \kappa\phi)\tilde{\Delta}_{i+1}^-\right) \qquad (7)$$

where ϕ represents a flux limiter, which for our study was that developed by Anderson *et al* [12]. Equations (6) and (7) thus represent a modified MUSCL scheme for non-uniform grids, based on a quadratic distribution of U across the cell. If the grid is uniform then $r_i^{\pm}=1$, and the original MUSCL scheme is recovered.

The modified MUSCL scheme was employed on grid 6. Figure 8 presents the crossflow solution at $x/D=8$ and clearly demonstrates the dramatic improvement the modified MUSCL scheme produced. The numerical shear layer and the associated vortices, which did appear as intermediate solutions, were convected out of the solution as it converged down by five orders. The final solution was comparable, even better, than the standard third-order MUSCL solution on the Euler grid (grid 1) despite the large cell stretching.

A further computation was performed, employing the modified MUSCL scheme on grid 5. This time the numerical boundary layer and resultant phantom vortices appeared only as an intermediate solution and disappeared as the solution converged down to five orders.

A final test was carried out using grid 5 to obtain a laminar solution with both the standard and the modified MUSCL scheme. The results, converged by five orders, were practically equivalent. This indicates that the phantom vorticity is much less of a problem for viscous

calculations; the physical dissipation being much greater than numerical.

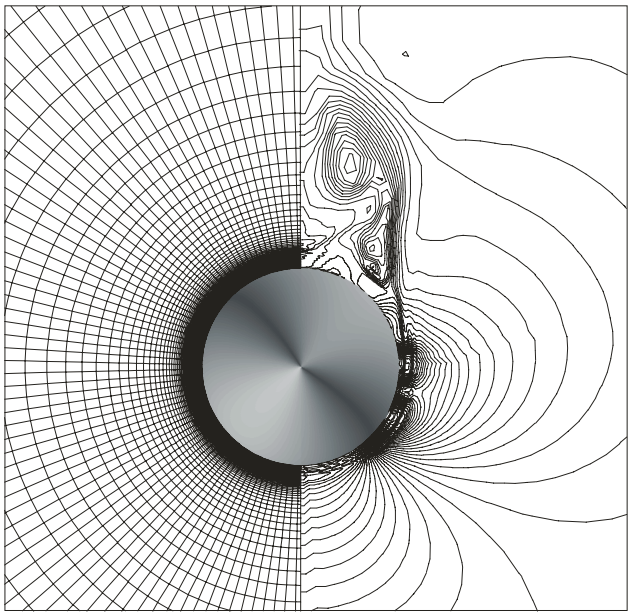

a) Pitot pressure contours and crossflow plane grid.

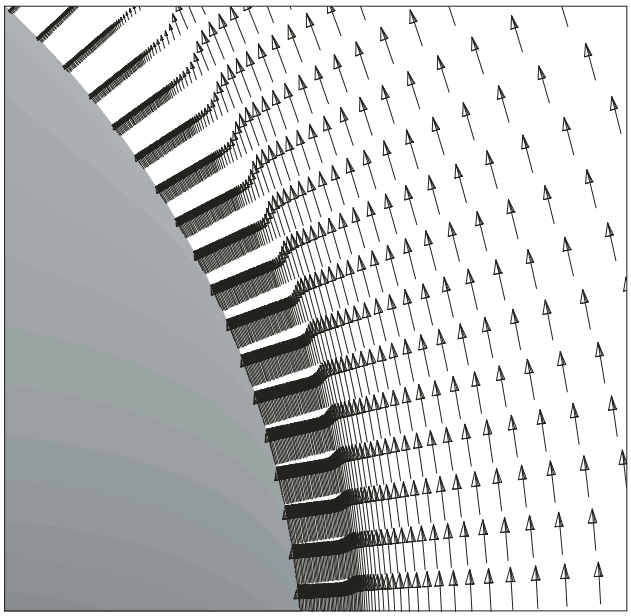

b) Crossflow velocity vectors

Figure 7: Euler third-order solution using standard MUSCL scheme.

6 Phantom Vorticity: Conclusions

The phenomenon of "phantom vorticity" in Euler solutions of the supersonic flow past smooth inclined slender bodies is linked with the spatial accuracy of the scheme, highly stretched grids, and to convergence problems.

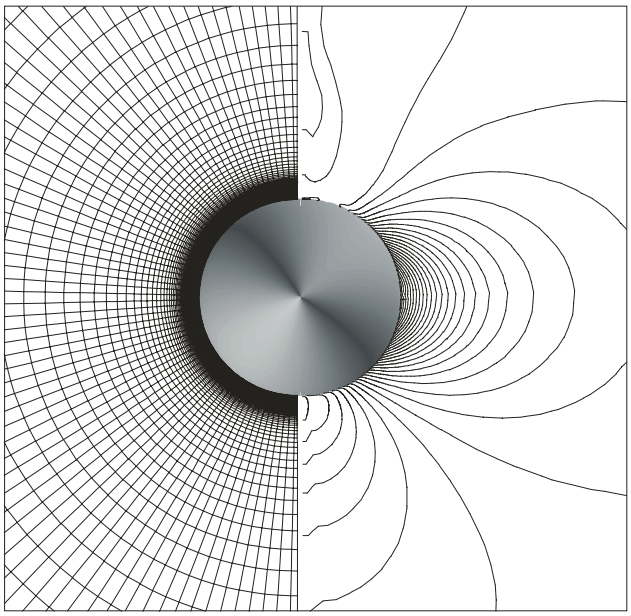

a) Pitot pressure contours and crossflow plane grid.

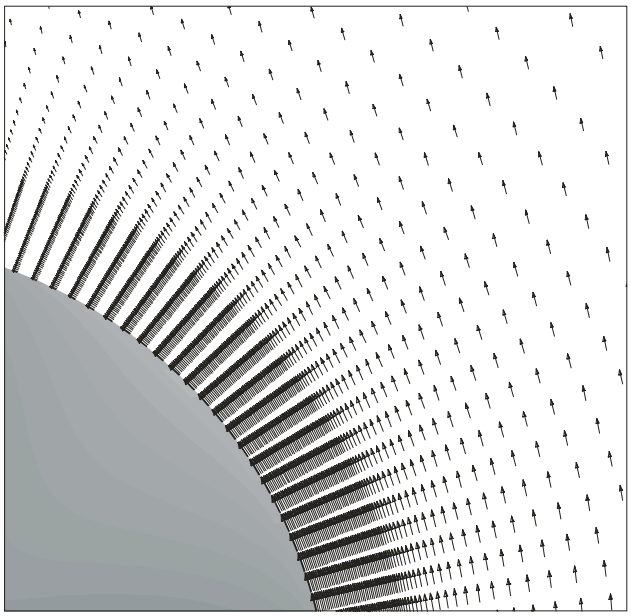

b) Crossflow velocity vectors

Figure 8: Euler third-order solution using modified MUSCL scheme.

The phenomenon was found to be independent of the implementation of the Euler slip boundary condition and of the use of either the Roe or Osher approximate Riemann solver.

This suggests that the phantom vorticity is generated by the excessive numerical dissipation associated with the localized loss of spatial accuracy in regions where the grid is highly stretched. Schemes that do not account for non-uniformity of the grid cannot maintain high order spatial accuracy and introduce excessive numerical dissipation that is localized to the highly stretched region of the grid. The Euler equations, having no mechanism for diffusion, cannot delocalize these errors which can only convect through the flow-field in the streamwise direction. Since the source of the numerical dissipation – highly stretched grids with an inconsistent scheme – remains as the flow develop, more and more numerical dissipation is generated and eventually the solution cannot converge any further.

Application of a scheme that accounts for grid non-uniformity will maintain higher order spatial accuracy in highly non-uniform regions of the mesh. The fact that phantom vorticity does occur but dies away as the solution is converged beyond three orders indicates that there is still a localized loss of spatial accuracy, but the resulting numerical dissipation is not strong enough to stall convergence.

The equivalence of the laminar solutions on a highly stretched grid using both formulations of the MUSCL scheme shows that any numerical dissipation is effectively dispersed by physical viscosity. With no localized errors, the solution is able to converge correctly down by five orders.

Acknowledgments

This work was funded by the UK Engineering and Physical Sciences Research Council and the Defence Evaluation Research Agency (DERA, UK Ministry of Defence). The authors are indebted to Trevor Birch of DERA for bringing the phenomenon of phantom vorticity to their attention and providing invaluable advice.

References

[1] Marconi F. Conical Separated Flows with Shock and Shed Vorticity. *AIAA Journal*, Vol. 25, No. 1, Jan. 1987, pp 173-175.

[2] Prince SA. *The Aerodynamics of High Speed Aerial Weapons.* PhD Thesis, Cranfield University, September 1999.

[3] Kwong CM, Myring DF and Livesey JL. Euler Calculations of Flow Round a Missile at High Alpha. *Departmental Report*, Salford University, Dec. 1990.

[4] Chinilov A. On Numerical Boundary Layers of Numerical Schemes Applied to Euler Equations. *Proceedings of the Seventh International Symposium on Computational Fluid Dynamics*, Beijing, pp 84-90, 1997.

[5] Turkel E. Accuracy of Schemes with Nonuniform Meshes for Compressible Fluid Flows. *Applied Numerical Mathematics 2*, North-Holland Publishing, pp 529-550, 1996.

[6] Batina JT. Implicit Flux-Split Schemes for Unsteady Aerodynamic Analysis Involving Unstructured Meshes. *AIAA Paper 90-0936-CP*, 1990.

[7] Batina JT. A Fast Implicit Upwind Solution Algorithm for Three Dimensional Unstructured Dynamic Meshes. *AIAA Paper 92-0447*, 1992.

[8] Liou M-S and Hsu AT. A Time Accurate Finite Volume High Resolution Scheme for Three Dimensional Navier-Stokes Equations. *AIAA Paper 89-1994-CP*, 1989.

[9] Qin N and Foster GW. Computational Study of Supersonic Lateral Jet Flow Interactions, *J. Spacecraft and Rockets*, Vol. 33, No 5, pp 651-656, 1996.

[10] Barberis D. Supersonic vortex flow around a missile body. *AGARD Advisory Report 303*, Vol. 2, Aug. 1994.

[11] van Leer B. Upwind-difference Methods for Aerodynamic Problems Governed by the Euler Equations. *Lecture Notes in Applied Mathematics*, 22:327-336, 1985.

[12] Anderson W, Thomas JL and van Leer B. Comparison of Finite Volume Flux Vector Splittings for the Euler Equations. *AIAA Journal* 24:1453-1460, 1986.